Science and Technology Indonesia
e-ISSN:2580-4391 *p*-ISSN:2580-4405
Vol. 11, No. 2, April 2026

Research Paper

ZnO-SiO_2 Nanocomposite: Synthesis, Characterization, and Application of Corrosion Inhibition

Alam Q. AL-Hussin[1], Ali Taleb Bader[1*], Hazim Yahya Al-Gubury[1]

[1]*Department of Chemistry, College of Science for Women, University of Babylon, Hilla, 51001, Iraq*
***Corresponding author**: wsc.ali.taleb@uobabylon.edu.iq*

Abstract
Herein, we report the synthesis of zinc oxide (ZnO), silicon dioxide (SiO_2), and a binary nanocomposite ZnO-SiO_2 via the co-precipitation method. The synthesized materials were comprehensively characterized, using via Fourier-transform infrared spectroscopy (FTIR), scanning electron microscopy (SEM), powder X-ray diffraction (XRD), UV-Vis spectroscopy, and nitrogen adsorption-desorption (BET) measurements prior to their application. The presence of typical Zn-O and Si-O vibrations characteristic of ZnO was confirmed by FTIR spectra, while the hexagonal morphology of ZnO crystals, spherical nature of SiO_2, and agglomerated structure of the ZnO-SiO_2 nanocomposite were confirmed by SEM images. XRD analysis confirmed the crystallinity of the as-obtained nanostructures, with average crystallite sizes of 37.78 nm (ZnO), 48.01 nm (SiO_2), and 34.09 nm nanocomposite (ZnO-SiO_2), as calculated using the Scherrer equation. The synthesized ZnO, SiO_2, and ZnO-SiO_2 nanoparticles were then evaluated on the basis of their inhibitive abilities toward corrosion processes in mild steel coupons exposed to 1M HCl estimated by potentiodynamic polarization. All the studied binary composites emerged as having the strongest inhibitory potential, with the ZnO-SiO_2 nanocomposite root system experience showing the most powerful inhibition potential, reducing the corrosion current density (i-corr) to 36.1 $\mu A \cdot cm^{-2}$ and achieving an inhibition efficiency of 93%. These results demonstrate that the future of using co-precipitation-is a promising method for synthesizing tunable nanocomposites with desirable physicochemical properties for efficient corrosion inhibition in acidic media.

Keywords
Nanocomposite, ZnO-SiO_2 Nanocomposite, Corrosion Inhibition, Mild Steel

Received: 17 August 2025, Accepted: 19 January 2026
https://doi.org/10.26554/sti.2026.11.2.538-550

1. INTRODUCTION

The recent scientific technological advancement has propelled nanotechnology to the forefront of scientific inquiry, particularly in its capacity to revolutionize diverse biomedical and technological domains (Nam and Luong, 2019). Nanomaterials, especially nanoparticles (NPs), are known for their unparalleled optical, electronic, and catalytic properties, which are intrinsically linked to their extraordinarily high surface-area-to-volume ratio (Mishra et al., 2017). This unique characteristic underpins their enhanced reactivity and efficiency compared to their bulk counterparts. Consequently, metal-based and metal oxide-based nanoparticles have created immense research interest over the past two decades, emerging as foundational elements in numerous cutting-edge applications (Chen et al., 2022a).

Among the myriads of metal oxide nanoparticles, zinc oxide nanoparticles (ZnO NPs) stand out as a highly prominent class due to their remarkable multifunctionality, natural abundance, and cost-effectiveness (Dey et al., 2025; Divya et al., 2018) As an n-type II-VI semiconductor, ZnO possesses a wide direct band gap of approximately 3.3 eV and exhibits excellent chemical and thermal stability, alongside a large exciton binding energy. These attributes make ZnO NPs particularly attractive for a broad spectrum of applications, including advanced optoelectronics, highly sensitive sensors, and efficient photocatalysis (Chen et al., 2022a; Ghafouri et al., 2013; Top and Çetinkaya, 2015). However, a significant challenge inherent to ZnO nanoparticles is their strong propensity for agglomeration, primarily driven by high surface energy. This aggregation can severely impede their performance and limit the realization of their full potential in various applications (Chen et al., 2022b).

In parallel, silicon dioxide nanoparticles (SiO_2 NPs) have been extensively investigated for their compelling properties, which include low toxicity, inherent biocompatibility, chemical inertness, and facile surface functionalization with a wide array of polymers and biomolecules (Bahmani et al., 2014; Dubey

et al., 2015; Thirumalaivasan et al., 2025). These advantageous characteristics position SiO_2 NPs as indispensable materials in polymer science, advanced materials engineering, and critical biomedical applications. Crucially, the strategic incorporation of SiO_2 into ZnO matrices offers a potent solution to the agglomeration issue faced by ZnO NPs. SiO_2 functions as an effective support matrix, which not only mitigates ZnO particle growth but also significantly reduces aggregation, thereby leading to an enhancement in the available surface area and optimizing the catalytic interface (Ali et al., 2014; Krishnakumar et al., 2017). The synergistic interplay between ZnO and SiO_2 in the resulting ZnO-SiO_2 nanocomposites frequently translates into superior physicochemical properties, encompassing improved structural stability, augmented mechanical strength, and enhanced corrosion resistance (Rahmat et al., 2021).

The synthesis of ZnO-SiO_2 nanocomposites typically employs liquid-phase methods, such as solid dispersion, sol-gel processes, and co-precipitation techniques, which offer precise control over morphology and particle size (Babu et al., 2014; Krishnakumar et al., 2017; Li et al., 2023; Nguyen et al., 2024; Samuel et al., 2025). The goal of incorporating SiO_2 within ZnO matrices is to achieve substantially enhanced performance in catalytic, biomedical, and protective applications. While the literature extensively discusses the individual properties and some combined applications, there remains a need for a more comprehensive understanding of their tailored application in specific industrial challenges, particularly concerning durable corrosion inhibition.

Corrosion represents a pervasive and critical challenge that spans vital industrial sectors such as construction, transportation, energy, and marine industries. It leads to profound structural degradation, significant economic losses, and poses severe environmental and safety hazards (Gupta et al., 2023b; Prošek et al., 2025). Traditional corrosion inhibitors often rely on hazardous chemicals, which necessitates an urgent paradigm shift towards greener, more efficient, and sustainable alternatives. Nanomaterials, especially metal oxide-based nanocomposites, present a highly promising candidiate for advanced corrosion protection. They function by forming uniform, highly adherent, and robust protective layers on metal surfaces, thereby significantly enhancing material durability and extending service life (A. and Xavier, 2025; Aslam et al., 2020).

While the synergistic benefits of ZnO-SiO_2 nanocomposites are acknowledged, a critical research gap exists in systematically optimizing their anti-corrosive performance on mild steel substrates, particularly through a well-controlled co-precipitation route that emphasizes tailored morphology for enhanced surface adhesion and barrier properties. Existing studies often focus on general catalytic or biomedical applications, with less emphasis on a detailed electrochemical assessment of their long-term corrosion inhibition capabilities in challenging environments or the precise correlation between synthesis parameters and inhibition efficiency for mild steel. Furthermore, there is a limited number of recent investigations that thoroughly characterize the structural and morphological evolution of such nanocomposites synthesized via a controlled co-precipitation method, and then directly link these characteristics to their performance as a protective coating on mild steel through comprehensive electrochemical techniques.

This current work addresses this gap by presenting a novel approach for the synthesis of a ZnO-SiO_2 nanocomposite using a precisely controlled co-precipitation method, aimed at achieving optimal structural integrity and dispersion. The synthesized nanocomposite is rigorously characterized using a suite of advanced analytical techniques, including Fourier-transform infrared spectroscopy (FTIR), X-ray diffraction (XRD), scanning electron microscopy coupled with energy-dispersive X-ray spectroscopy (SEM/EDS), and Ultraviolet-visible spectroscopy (UV-Vis). The primary novelty of this study lies in its detailed assessment of the corrosion inhibition performance of this ZnO-SiO_2 nanocomposite on a mild steel substrate. By precisely correlating the nanocomposite's structural and chemical properties with its protective capabilities, this research aims to unequivocally demonstrate the potential of ZnO-SiO_2 nanocomposites as highly efficient, environmentally benign, and sustainable corrosion inhibitors, offering a significant advancement over conventional hazardous alternatives.

2. EXPERIMENTAL SECTION

2.1 Material

All the chemical compounds used in this work were of high purity, and used as received without further purification. These include $Zn(CH_3COOH)_2$ (Merck, Germany), NaOH (CDH, Indian), sodium silicate pentahydrate ($Na_2SiO_3.5H_2O$) (Thomas Baker, Indian), and hydrochloric acid HCL (Merck, Germany).

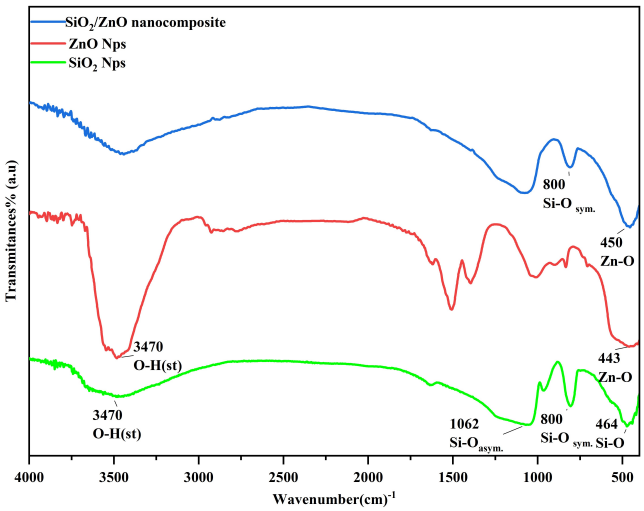

Figure 1. FTIR Spectra of SiO_2, ZnO and ZnO-SiO_2 Nanocomposite

2.2 Characterization Instruments

Fourier-transform infrared (FT-IR) spectroscopy was employed to characterize the structural and functional groups of the com-

pounds on a Shimadzu's FT-IR spectrophotometer (Model: 8400S) with an attenuated total reflection (ATR) accessory over a spectral range of 4000-400 cm^{-1}. At the same time, UV-Vis absorption spectra that provide information about optical properties of the compound to be studied were also collected, using a Shimadzu UV-Vis spectrophotometer (Model: 1700) at room temperature (r.t.) in the wavelength range 200-1100 nm using a 1 cm quartz cell. The final products were calcined post-synthesis in a Carbonite S336RB furnace (England). Instrumental measurements were available at the University of Babylon, College of Science for Women. Surface morphology of ZnO nanoparticles was investigated by use of a scanning electron microscope (SEM, Zeiss, Germany) at the University of Tehran, equipped with energy-dispersive X-ray spectroscopy (EDS) for elemental analysis. X-ray diffraction (XRD) data were collected on an X-ray diffractometer (Shimadzu XRD-6000, Japan) at the Ministry of Science and Technology. Furthermore, nitrogen adsorption-desorption isotherms at 77 K to determine by the BET surface area and pore characteristics.

2.3 Methods

2.3.1 Synthesis of SiO_2 Nanoparticles

Silicon dioxide (SiO_2) nanoparticles were synthesized by precipitation methods. Sodium silicate (Na_2SiO_3) was dissolved in distilled water at a molar ratio of 1:2 and stirred for 4 hours. The solution was titrated dropwise into 1 M hydrochloric acid (HCl) with continuous stirring at room temperature until the pH dropped from 12 to 7, resulting in the precipitation of a white solid. To remove excess acid, the precipitate was washed thoroughly with distilled water to remove excess acid, and the precipitate was then dried at 60 °C for 12 hours (Joni et al., 2020; Kumar Yadav and Fulekar, 2019; Yang et al., 2019).

2.3.2 Synthesis of ZnO Nanoparticles

Synthesis of ZnO nanoparticles was achieved by chemical co-precipitation method. A solution of deionized water and zinc acetate ($Zn(CH_3COO)_2$) of analytical quality was used as the solvent. 0.3 M NaOH was added dropwise to a 0.07 M zinc acetate solution (200 mL) until a white precipitate was formed. After filtration and washing with deionized water the precipitate was dried at 110 °C for 12 hours. The resulting powder was ground and calcined at 400 °C for 2 hours to improve its crystallinity (Adam et al., 2018; Justine et al., 2021; Raza et al., 2025).

2.3.3 Synthesis of SiO_2/ZnO Nanocomposite

The SiO_2/ZnO nanocomposite was prepared by in-situ co-precipitation method. Approximately 0.104 g of the as-synthesized SiO_2 nanoparticles were dispersed in 236 mL deionized water via probe sonication for 10 minutes. The dispersion was then added to 200 mL of 0.07 M zinc acetate solution under constant stirring. The pH of the mixture was adjusted to 8 via dropwise addition of 0.3 M NaOH, followed by overnight stirring at ambient temperature which afforded a white precipitate. The precipitate was washed with water, and dried at 110 °C for 48 hours. Finally, the powder was ground and calcined at 400 °C for 2 hours to improve crystallinity and complete nanocomposite formation (Chen et al., 2017; Yang et al., 2008).

2.3.4 Corrosion Testing of SiO_2, ZnO and SiO_2/ZnO Nanocomposite

Electrochemical corrosion studies were conducted using a PalmSens EmStat4s potentiostat/Galvano stat integrated with a magnetic stirrer and a thermostat to maintain 298 K. A 250 mL double-jacketed Pyrex cell with a three-electrode setup was used: carbon steel sheet (as the working electrode), platinum wire (counter electrode), and a saturated calomel electrode (SCE, reference electrode) . Prior to Tafel polarization measurements, the working electrode was immersed in the test solution to allow the open-circuit potential (EOCP) to stabilize for 15 minutes. Potentiodynamic Polarization scans were recorded over ±200 mV relative to EOCP. A circulating water bath ensured constant temperature control throughout the experiments (Gupta et al., 2023a; Raji and Bader, 2025).

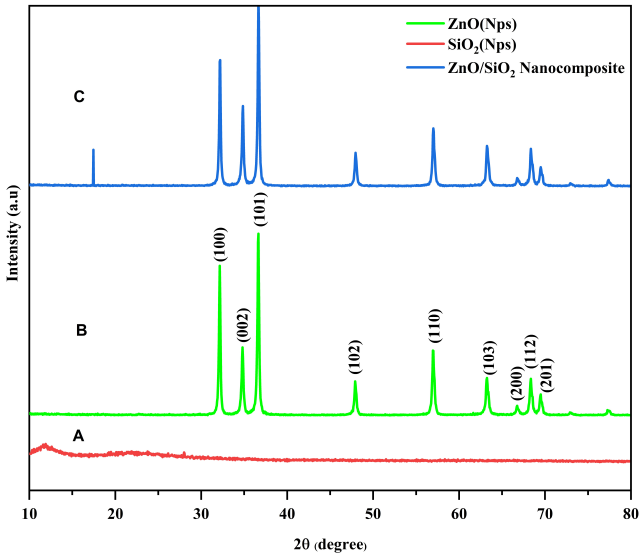

Figure 2. The X-Ray Diffraction (XRD) Patterns for SiO_2 (A), ZnO (B), and the SiO_2/ZnO Nanocomposite (C) are Presented

3. RESULT AND DISCUSSIONS

3.1 FTIR Spectra for SiO_2, ZnO Nanoparticular and SiO_2/ZnO Nanocomposite

The FTIR spectrum of the synthesized SiO_2 nanoparticles is shown in Figure 1 and Table 1. It displays distinct vibrational modes that confirm the successful synthesis of nanoscale silica. A broad absorption band is observed at approximately 3480 cm^{-1} which is attributed to the O−H stretching vibration from the hydroxyl groups on the nanoparticle surface and the adsorbed moisture. This is a common characteristic of nanomaterials with a large surface area. A peak near 1616

Table 1. FTIR Spectral Data for SiO_2, ZnO Nanoparticles and SiO_2/ZnO Nanocomposite

Wavenumber (cm^{-1})	Assignment	Sample(s)	Explanation
~ 3470	O–H stretching (νO–H)	All samples	Broad band due to surface hydroxyl groups or adsorbed water (Sukhov et al., 2024)
1610–1614	O–H bending (δH–O–H)	All samples	Bending vibration of H–O–H from water molecules (Heinhold et al., 2013)
1500, 1400	COO^- asymmetric and symmetric stretching	ZnO, nanocomposite	Suggests presence of carboxylate (–COOH) or adsorbed organic residues (Andrade-Guel et al., 2022)
~1062	Si–O–Si asymmetric stretching ($\nu Si–O_{asym}$)	SiO_2, nanocomposite	Indicates a silica network, which is more intense in SiO_2 (Liang et al., 2012)
~ 800	Si–O symmetric stretching ($\nu Si–O_{sym}$)	SiO_2	Typical of amorphous silica
464–443	Zn–O stretching	ZnO, nanocomposite	Confirms presence of ZnO wurtzite structure (Ajobree et al., 2019)

cm^{-1} is assigned to the H–O–H bending mode of physiosorbed water. The intense band located at approximately 1026 cm^{-1} corresponds to the asymmetric stretching vibration of Si–O–Si bridges, a key fingerprint of silica networks. A shoulder at around 837 cm^{-1} reflects symmetric Si–O stretching, and the band near 474 cm^{-1} corresponds to Si–O bending vibrations (Dhaffouli et al., 2024).

Similarly, Figure 1 shows the FTIR spectrum of the synthesized ZnO nanoparticles. A wide absorption band is observed in the spectrum at 3470 cm^{-1}, attributed to the OH stretching vibrations of the hydroxyl groups and the water molecules adsorbed on the nanoparticle surface. Additionally, a band at approximately 1614 cm^{-1} corresponds to the H–O–H bending mode, further confirming the presence of physisorbed water. Weak absorption bands in the region of 1400-1500 cm^{-1} region are associated with the asymmetric and symmetric stretching of carboxylate groups, likely from residual acetate precursors.

A small peak observed near 1000 cm^{-1} may be attributed to C–O stretching vibrations, which could indicate the presence of minor organic residues or surface adsorbents species. Most importantly, a prominent and sharp absorption band in the region of 443cm^{-1} is clearly observed. This peak is characteristic of the Zn-O stretching vibration, confirming the formation of ZnO nanoparticles (S. et al., 2020). The presence of this band is considered a fingerprint for ZnO structures, and its appearance strongly supports the successful synthesis of crystalline ZnO.These results confirm the formation of ZnO nanoparticles with surface hydroxylation and minimal organic contamination, typical of ZnO produced via solution-based synthesis routes (S. et al., 2020). Combines all major vibrational modes from both SiO2 and ZnO. Notably, the characteristic Zn-O band is retained at 443 cm^{-1}, while the Si–O–Si stretching band also persist, indicating the physical integration of both phases. A slight shift in the Zn-O band within the composite spectrum suggests an interaction at the ZnO-SiO_2 interface, possibly through hydrogen bonding between surface hydroxyl groups.

3.2 XRD Patterns for ZnO, SiO_2, and ZnO/SiO_2

Figure 2 (A, B, C) shows X-ray diffraction (XRD) patterns for ZnO nanoparticles, SiO_2 nanoparticles , and a ZnO/SiO_2 nanocomposite In the ZnO pattern several sharp and intense diffraction peaks are observed at approximately 2θ = 31.8°, 34.5°, 36.3°, 47.5°, 56.6°, 62.8°, 67.9°, and 69.1°, which correspond to the (100), (002), (101), (102), (110), (103), (200), (112)/(201) planes, respectively. These diffraction peaks correspond to the hexagonal wurtzite structure of ZnO (JCPDS Card No. 36-1451), indicating high crystallinity (Ahsbahs and Sowa, 2006; Subhi et al., 2022). In contrast, the XRD pattern of the synthesized SiO_2 nanoparticles feature a broad, diffuse hump centered at approximately $2\theta \approx 21°$, which is characteristic of an amorphous structure. This board hump arises in short-range ordering of Si–O–Si networks but the absence of long-range periodicity typical in crystalline materials. No sharp diffraction peaks were observed, which rules out the presence of crystalline phases such as quartz, cristobalite, or tridymite. The background noise beyond 30° suggests random atomic arrangements without significant periodicity (Yang et al., 2019).

The XRD pattern of the ZnO/SiO_2 nanocomposite (blue curve in Figure 2C) reveals key insights into the phase structure and crystallinity of the hybrid material. The composite shows sharp diffraction peaks at 2θ = 31.7°, 34.4°, 36.2°, 47.5°, 56.6°, 62.9°, 66.4°, and 68.0°, which corresponds to the (010), (002), (011), (012), (110), (013), (112), and (021) planes of hexagonal wurtzite ZnO (JCPDS card No. 36-1451), confirming that the ZnO retains its crystalline phase within the composite. These peaks are identical to those seen in the pure ZnO sample (green curve), indicating that the crystallinity of ZnO is preserved upon incorporation into the silica matrix. The absence of additional peaks related to any new phases or compounds suggests that the ZnO and SiO_2 did not chemi-

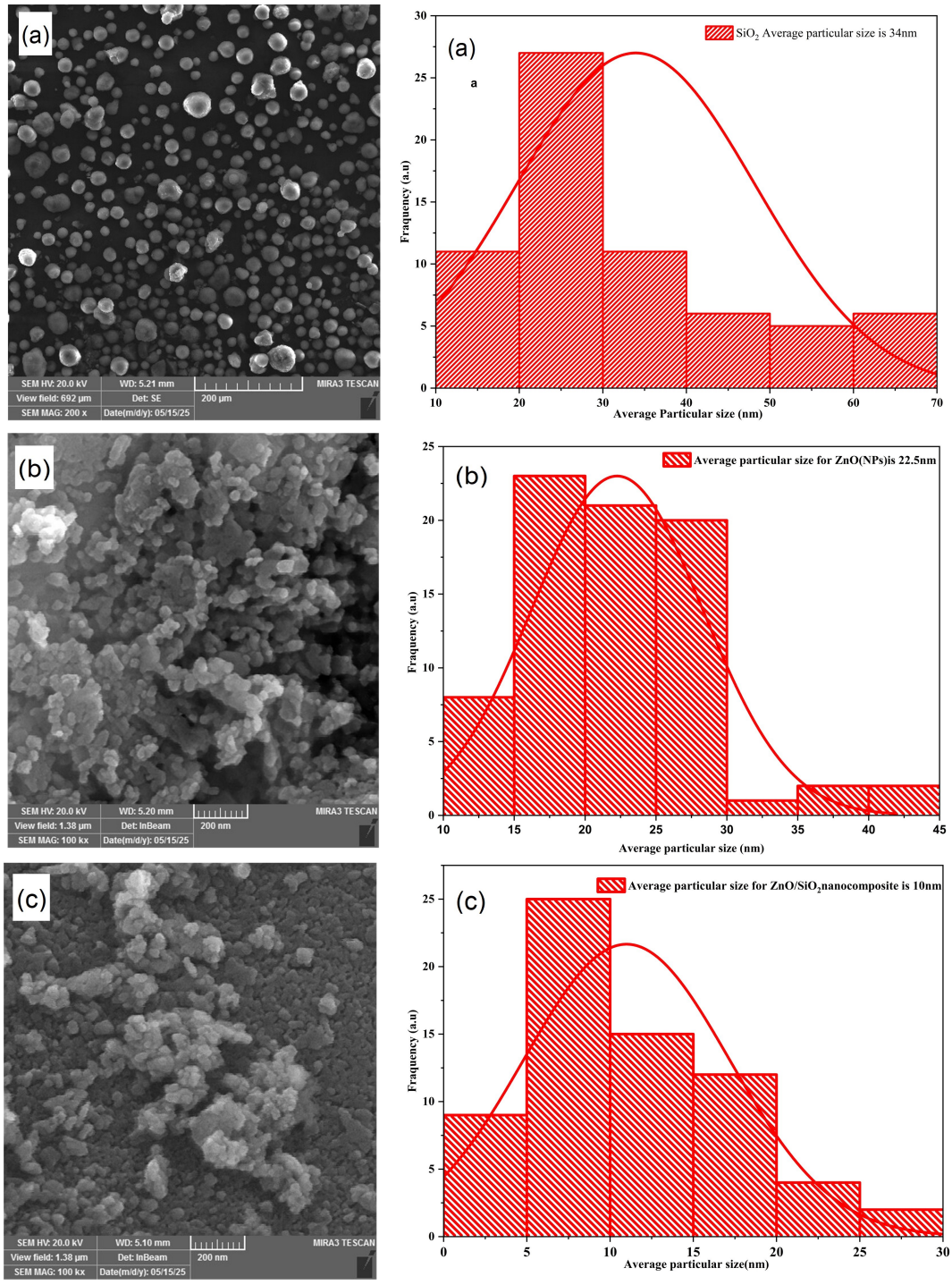

Figure 3. Scanning Electron Microscopy (SEM) Micrographs and Particle Size Distribution SiO_2 Nps (a), ZnO Nps (b) and SiO_2/ZnO Nanocomposite

cally react to form a new crystalline structure but rather formed a physical nanocomposite, where ZnO nanoparticles are embedded or dispersed within the amorphous SiO_2 framework. This conclusion is supported by the lack of sharp peaks in the SiO_2 pattern (red curve), which only displays a broad hump around 22° 2θ-typical of amorphous silica. Notably, the ZnO diffraction peaks in the nanocomposite are slightly broader and less intense compared to pure ZnO. This peak broadening

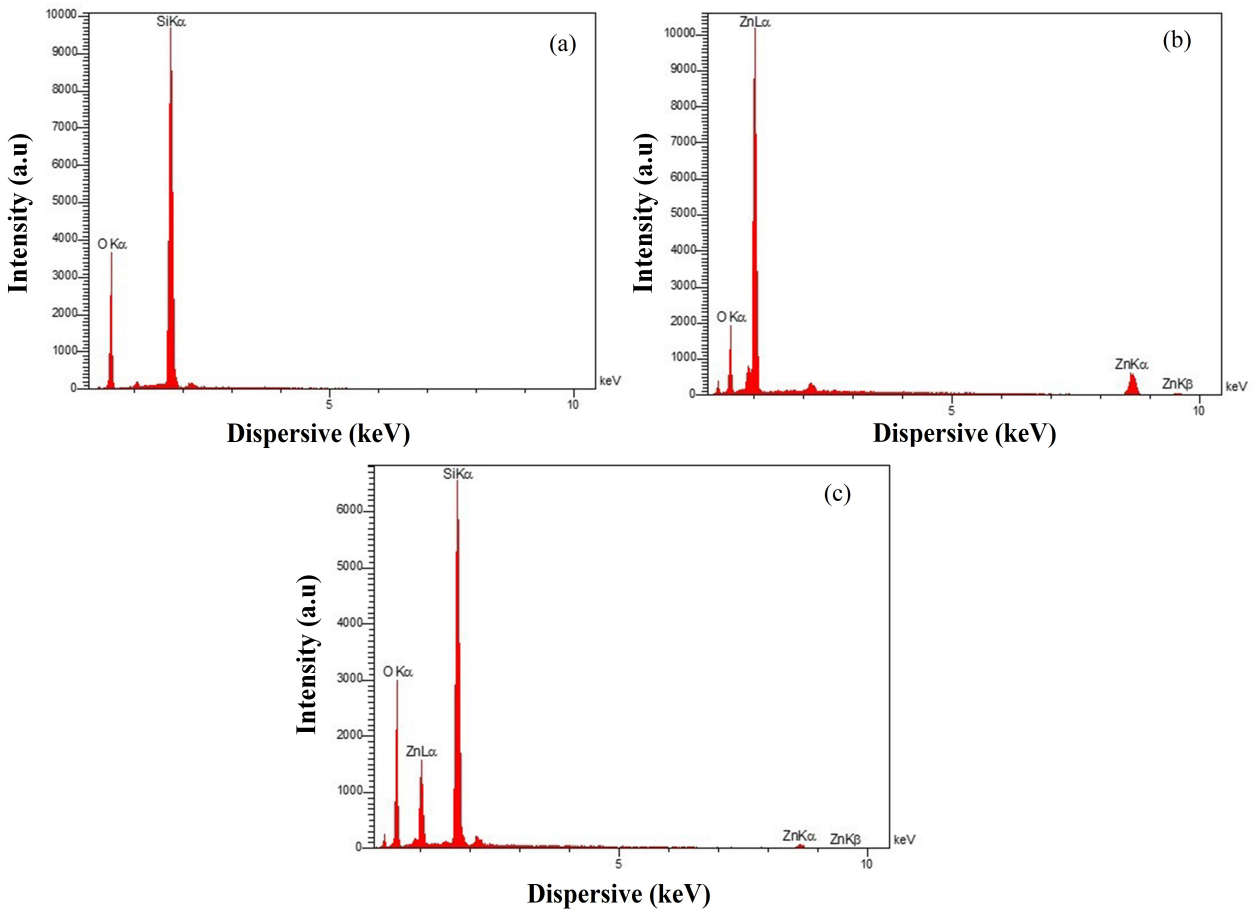

Figure 4. Energy-Dispersive X-Ray (EDX) Spectra of SiO_2 Nps (a), ZnO Nps (b), and SiO_2/ ZnO Nanocomposite (c)

Table 2. EDX Elemental Composition of SiO_2, ZnO and ZnO/SiO_2 Nanocomposite

Element	Line	Int	Error	K	Kr	Wt%	At%	ZAF	Ox%	Pk/Bg
O	Ka	915.8	11.4245	0.4062	0.2506	56.16	69.22	0.4462	0.00	862.17
Si	Ka	3652.3	14.5975	0.5938	0.3664	43.84	30.78	0.8358	0.00	103.51
				1.0000	0.6170	100.00	100.00		0.00	
O	Ka	486.6	26.9685	0.1579	0.1281	25.39	58.17	0.5046	0.00	238.47
Zn	Ka	546.8	0.9960	0.8421	0.6833	74.61	41.83	0.9158	0.00	39.23
				1.0000	0.8114	100.00	100.00		0.00	
O	Ka	759.5	14.5662	0.4049	0.2473	53.67	69.43	0.4608	0.00	684.60
Si	Ka	2494.6	3.1893	0.4875	0.2978	37.82	27.87	0.7873	0.00	64.57
Zn	Ka	42.5	1.0269	0.1075	0.0657	8.51	2.69	0.7719	0.00	7.19
				1.0000	0.6108	100.00				

implies reduced crystallite size and/or lattice strain, likely due to nanoconfinement effects or interaction at the ZnO/SiO_2 interface. Such microstructural refinement is known to improve surface activity, increase defect density, and enhance properties like photocatalytic performance, corrosion resistance, and interfacial adhesion in coatings (Fatimah et al., 2021). The average crystallite size (D) was calculated from the most intense diffraction peak (101) using the Debye-Scherrer equation:

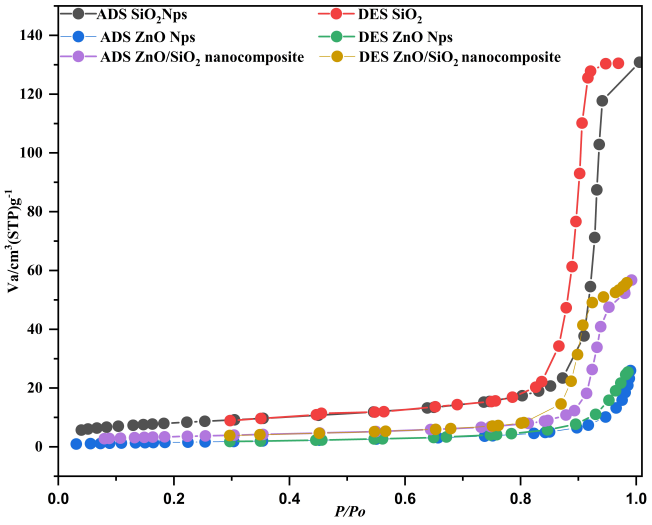

Figure 5. Nitrogen Adsorption (ADS)-Desorption (DES) Isotherms of SiO_2 Nanoparticles, and ZnO Nanoparticles and SiO_2/ZnO Nanocomposite at 77 K

$$D = \frac{K\lambda}{\beta \cos\theta} \quad (1)$$

The calculated average crystallite sizes for ZnO and the ZnO/SiO_2 nanocomposite were 37.78 nm and 34.09 nm, respectively.

3.3 Field Emission Scanning Electron Microscopy (FESEM) Characterization for SiO_2, ZnO and SiO_2/ZnO Nanocomposite

The surface morphology of the synthesized materials was investigated by SEM (Figure 3 (a,b.c). The SEM micrograph of SiO_2 nanoparticles (Figure 3a reveals a quasi-spherical morphology with a significant tendency to form agglomerates, which is typical for nanoscale silica due to high surface energy. The particle size distribution (Figure 3a) is unimodal, with an average particle size of approximately 34 nm. The ZnO nanoparticles (Figure 3b) also exhibit a quasi-spherical to irregular shape with cluster formation. Their average particle size is approximately 22.5 nm (Figure 3b).

The SEM image of the ZnO-SiO_2 nanocomposite (Figure 3c) shows ZnO nanoparticles dispersed on the SiO_2 matrix. Compared to pure ZnO, the nanocomposite exhibits reduced particle agglomeration, indicating that the SiO_2 matrix acts as an effective support and dispersing medium. The particle size distribution for the nanocomposite (Figure 3c) shows an average particle size of approximately 10 nm, which is smaller than either of the individual components, supporting the XRD finding of reduced crystallite size.

3.4 EDX Characterizations

Elemental analysis by energy-dispersive X-ray spectroscopy (EDX) was performed on pure SiO_2, ZnO, and the SiO_2/ZnO nanocomposite (see Figures 4 (a,b,c) and Table 2). Results confirm the successful incorporation of ZnO into the SiO_2 matrix are presented below. EDX spectrum of the pure silica sample revealed the detection of only silicon, and oxygen, with a weight percentage close to the theoretical ratio of SiO_2. The atomic percentages (Si ~30.78%, O ~69.22%) confirm the expected 1:2 ratio (Si:O), suggesting the formation of stoichiometric silica with high purity. No trace elements or metallic impurities were detected. Similarly, the ZnO sample showed strong signals for both Zn and O, with Zn contributing the majority of the mass (74.61% by weight). The atomic ratio is consistent with stoichiometric ZnO. The high Zn signal is due to its higher atomic weight compared to oxygen. These values confirm the successful synthesis of ZnO nanoparticles without contamination. The EDX spectrum for the ZnO-SiO_2 nanocomposite confirmed the presence of all three elements (Zn, Si, O), verifying the successful formation of the composite material. The weight percentage of Zn was 8.51%, indicating its dispersion within the silica matrix. The low atomic % of Zn (2.69%) confirms it is well-dispersed and possibly exists in nanocrystalline or quantum dot form within the silica structure. This supports the optical band gap widening observed in UV-Vis and Tauc plot analyses. The presence of Zn without other elements also confirms the chemical purity of the composite.

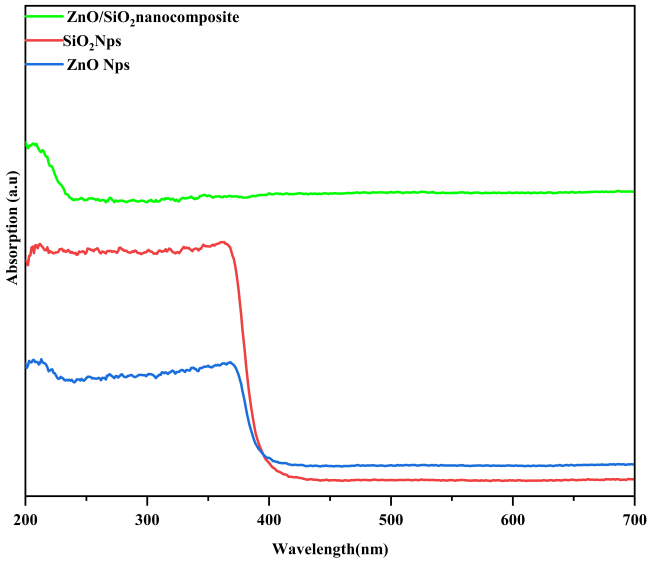

Figure 6. Electronic Transitions for SiO_2 Nanoparticles, ZnO Nanoparticles and SiO_2/ZnO Nanocomposite

3.5 Characterization of Surface area for ZnO, SiO_2 and ZnO/SiO_2 Nanocomposite

The specific surface area and pore morphology of the nanoparticles were determined using the Brunauer-Emmett-Teller (BET) method based on nitrogen adsorption-desorption isotherms, as presented in Figure 5. Nitrogen adsorption-desorption measurements were carried out to investigate the textural characteristics of the synthesized SiO_2 nanoparticles, ZnO

Table 3. BET Surface Area and the Porosity Data for SiO_2, ZnO and ZnO/SiO_2 Nanocomposite

Compound	Surface area ($m^2\ g^{-1}$)	Total pore volume ($cm^3\ g^{-1}$)	Mean pore diameter (nm)
SiO_2	29.159	0.1974	27.082
ZnO	5.8397	0.039 837	27.287
ZnO/SiO_2	12.578	0.086 761	27.591

nanoparticles, and the ZnO/SiO_2 nanocomposite. The isotherms presented in Figure 5 fit the IUPAC Type IV description and their strong H3-type hysteretic loops, which are features normally found to be typical of mesoporous structures with slit pore shapes (Huang et al., 2019). As shown in Table 3, pure SiO_2 nanoparticles exhibited the highest specific surface area (29.16 m^2/g) and total pore volume (0.197 cm^3/g). ZnO nanoparticles showed a much lower surface area (5.84 m2/g). The ZnO-SiO_2 nanocomposite had an intermediate surface area of 12.58 m^2/g (Subhi et al., 2022).

The formation of plate-like particle aggregates or assemblies of layered structures most commonly results in this sort of pore. At low relative pressures ($P/P0 < 0.4$), all samples display a gradual increase in nitrogen uptake, which is the indication of monolayer-multilayer adsorption on the pore walls. A steep increase in adsorption at high relative pressure ($P/P0 > 0.8$) signifies capillary condensation within mesopores, which is especially pronounced in the SiO_2 sample, reflecting its high porosity. Among the materials, pure SiO_2 nanoparticles exhibited the highest adsorption capacity, with a sharp nitrogen uptake and large total pore volume, confirming their well-developed mesoporous structure. The ZnO nanoparticles, on the other hand, showed a much lower adsorbed volume, indicating a lower surface area and limited mesoporosity. The SiO_2/ZnO nanocomposite demonstrated intermediate adsorption behavior. Although the incorporation of ZnO reduced the overall adsorption volume compared to pure SiO_2, the composite still retained a clear hysteresis loop and a mesoporous structure, confirming that ZnO nanoparticles was well dispersed within the silica matrix without collapsing the porous framework. The phenomenon of reduction of BET surface of composite has been previously reported by (Safavinia et al., 2021).

3.6 Optical Properties and Band Gap Analysis

In Figure 6, UV-Vis absorption spectra of SiO_2, ZnO, and the SiO_2/ZnO nanocomposite provide essential insights into their optical characteristics. Pure ZnO nanoparticles show exhibit a distinct absorption edge around 375 nm, which is typical for this wide-band-gap semiconductor (Singh et al., 2014; Zhang et al., 2010). In contrast, the SiO_2nanoparticles show minimal absorption due to their very large band gap (>9 eV). The SiO_2/ZnO nanocomposite spectrum maintains an absorption edge close to that of pure ZnO, but exhibits significantly enhanced overall absorbance in the UV region. However, the composite demonstrates significantly enhanced overall absorbance across the UV region relative to pure ZnO. This improvement can be attributed to multiple light scattering within the porous SiO_2 matrix and enhanced light capture resulting from the homogeneous distribution of ZnO nanoparticles throughout the SiO_2 framework (Grigorie et al., 2017).

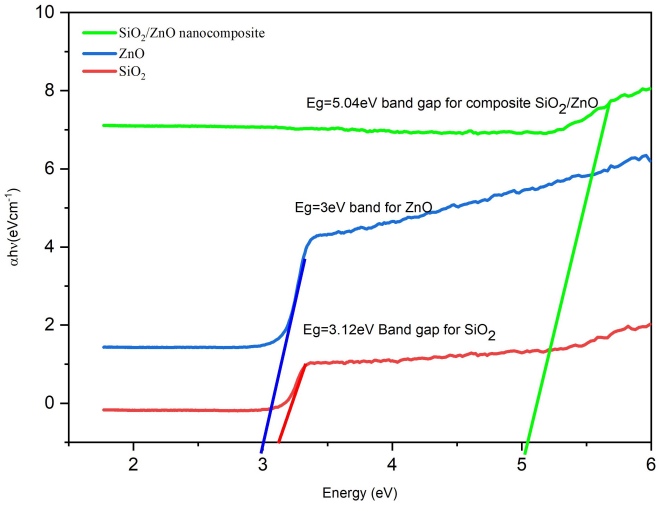

Figure 7. Band Gap Measurement for SiO_2 Nanoparticles, ZnO Nanoparticles and SiO_2/ZnO Nanocomposite

Additionally, the slight broadening observed in the absorption edge of the composite spectrum suggests the formation of interfacial defect states or shallow traps at the SiO_2-ZnO boundary. These localized states can modify the electronic environment, facilitating more effective electron-hole separation and thereby reducing recombination ratesan advantage for photocatalytic and optoelectronic applications (Zhang et al., 2008).Overall, these observations indicate that incorporating ZnO within a SiO_2 matrix not only preserves the intrinsic optical properties of ZnO, In addition leads to improved light absorption. This improvement underscore potential of SiO_2/ZnO nanocomposites for applications in photocatalysis, UV-blocking coatings, and other UV-responsive technologies (Ali et al., 2014). The optical properties of pure ZnO, pure SiO_2, and the SiO_2/ZnO nanocomposite were investigated using UV-Vis spectroscopy, and the corresponding Tauc plots are presented in the Figure 7 show the Tauc plots. The direct band gap energies were estimated via generalizing the linear portion

of the $(\alpha h\nu)^2$ versus photon energy curves to the energy axis using the Tauc relation (Tauc, 2012). The results indicate that pure ZnO exhibits a band gap of approximately 3.0 eV, which is consistent with previously reported values for bulk ZnO (Özgür et al., 2005). In contrast, the SiO_2 sample shows a band gap of around 3.12 eV, a little higher than ZnO but significantly lower than the theoretical band gap of bulk amorphous SiO_2 (~9 eV) (Tan et al., 2005) . This discrepancy may be attributed to surface defects, hydroxyl groups, or oxygen vacancies within the silica structure that introduce localized states (Skuja, 1998). Remarkably, the SiO_2/ZnO nanocomposite demonstrates a significantly increased band gap of 5.04 eV, reflecting a clear blue shift in the absorption edge. This enhancement ascribed to quantum confinement effects that arise when the ZnO particles are reduced to the nanoscale, resulting in discrete energy levels and a widening of the band gap (Brus, 1984; Spanhel and Anderson, 1991). Furthermore, the presence of the wide-band-gap SiO_2 matrix likely reduces interparticle interactions and minimizes defect-related states, leading to an overall improvement in optical purity and band structure (Torkian et al., 2024). These results confirm the successful formation of a nanocomposite with modified electronic properties. The high band gap value indicates that the SiO_2/ZnO nanocomposite is transparent in the visible region and primarily responsive to deep ultraviolet (DUV) light (Kamat, 2007).

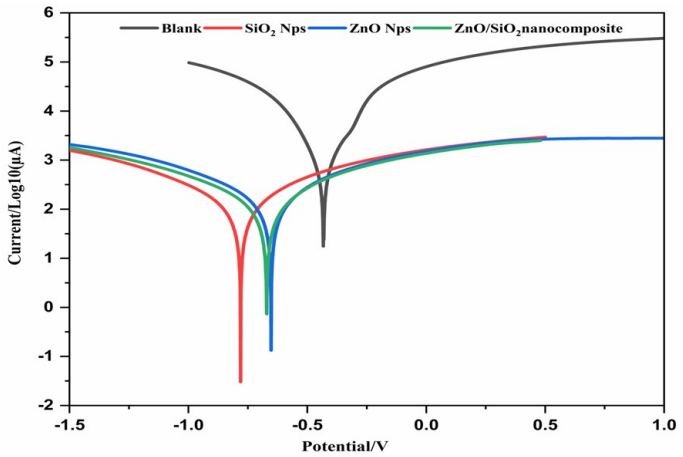

Figure 8. Tafel Curves Depicting Corrosion Behavior of Mild Steel with and without SiO_2, ZnO and SiO_2/ZnO Composite Coatings

3.7 Corrosion Inhibition Performance for SiO_2, ZnO and SiO_2/ZnO Nanocomposite

To determine the corrosion protection efficiency of the coatings, potentiodynamic polarization studies were performed on four different specimens: the uncoated substrate (blank) and the substrates coated with SiO_2, ZnO, and the SiO_2/ZnO nanocomposite. Electrochemical parameters measured in the current study, which include corrosion potential (E_corr), corrosion current density (i_corr), polarization resistance (R), Tafel slopes (B_a, B_c), corrosion rate, inhibition efficiency (IE %), and other parameters obtained during the corrosion process under the action of the inhibitor, are reported in Table 4. The uncoated sample exhibited the highest corrosion current density (icorr = 493.9 $\mu A/cm^2$) and corrosion rate (4.848 mm/y), indicating poor resistance to corrosion in the tested medium. In contrast, the samples coated with individual oxides (SiO_2 and ZnO) demonstrated significantly reduced icorr values (69.95 and 48.63 $\mu A/cm^2$, respectively), suggesting improved corrosion resistance. Most notably, the SiO_2/ZnO nanocomposite coating provided the best corrosion protection, with lowest i-corr of 36.11 $\mu A/cm^2$ and highest polarization resistance of 1982 Ω, which implies the formation of a highly protective surface layer.

Furthermore, the inhibition efficiency (IE%) of the coatings increased in the following order: SiO_2 (86%) < ZnO (90%) < SiO_2/ZnO (93%). The ZnO-SiO_2 nanocomposite demonstrated the highest inhibition efficiency (IE) of 93%, surpassing the individual efficiencies of both pure SiO_2 (86%) and ZnO (90%). The SiO_2 matrix acts as an impermeable, non-reactive protective shield which physically hinders the diffusion of corrosive ions through to the metallic substrate. Meanwhile, the embedded ZnO nanoparticles contribute to chemical protection by participating in surface passivation reactions, such as the formation of $Zn(OH)_2$ or ZnO films under electrochemical conditions. The uniform dispersion of ZnO within the silica matrix enhances coating compactness, reduces porosity, and eliminates defect sites that typically serve as corrosion initiation points. These combined effects result in reduced corrosion current density (i-corr) and improved polarization resistance, both of which are key indicators of high inhibition efficiency. Therefore, the high IE% of the nanocomposite reflects the improved protective behavior and structural integrity of the hybrid coating (Peng et al., 2023). Figure 8 shows the Tafel polarisation curves of mild steel under both non-corrosive and corrosive environments with the oxide protective layers namely, SiO_2, ZnO and a composite SiO_2/ZnO. These electrochemical parameters (Ecorr and i-corr) were used to determine the corrosion resistance behavior of each system.

The uncoated sample (Blank) displayed the highest i-corr value of 493.9 $\mu A/cm^2$ and an Ecorr of -0.427 V, indicating severe corrosion activity. Upon the application of pure SiO_2, the icorr decreased significantly to 69.95 $\mu A/cm^2$ and Ecorr shifted negatively to -0.761 V, suggesting improved corrosion resistance due to the physical barrier properties of SiO_2 (Corrales-Luna et al., 2019). Similarly, the ZnO-coated sample showed further improvement, with an icorr of 48.63 $\mu A/cm^2$ and Ecorr of -0.656 V. The ZnO layer likely contributes to corrosion mitigation through both physical coverage and the formation of a passivating Zn^{2+} based layer (Zhang et al., 2020).

Remarkably, the SiO_2/ZnO composite coating exhibited the best corrosion protection performance, with the lowest icorr of 36.11 $\mu A/cm^2$ and a slightly more positive Ecorr of -0.650 V compared to the ZnO alone. This synergistic improvement

Table 4. Electrochemical Corrosion Parameters of the Blank Mild Steel, and Pure SiO_2, pure ZnO, and SiO_2/ZnO Composite Samples Obtained from Tafel Polarization Measurements in Corrosive Media

Parameters	Blank	SiO_2	ZnO	SiO_2/ZnO Composite
E-corr (mV)	-0.427	-0.761	-0.656	-0.650
I-corr ($\mu A/cm^2$)	493.9	69.95	48.63	36.11
I-corr ($\mu A\ cm^{-2}$)	9.878×10^{-4}	1.399×10^{-4}	9.727×10^{-5}	7.222×10^{-5}
Resistance (Ω)	70.31	1735	1804	1982
B-c (mV/Dec)	0.156	0.526	0.362	0.306
Ba (mV/Dec)	0.164	0.596	0.457	0.357
Corrosion rate (mm/y)	4.848	0.687	0.477	0.354
Inhibition efficiency (IE)%	-	86	90	93

Table 5. Detailed Comparative Analysis of Corrosion Inhibition Performance

Coating System	Corrosion Density ($\mu A/cm^2$)	Inhibition Efficiency (IE %)	Key Findings
SiO_2/ZnO nanocomposite (Current study)	36.11	93	Exhibits Synergistic effect of SiO_2 matrix (physical barrier) and ZnO (chemical passivation). The resulting compact, defect-free protective layer superior to individual oxides. High polarization resistance confirms robust protection.
Epoxy + ZnO + SiO_2 NPs Abdus (Abdus Samad et al., 2020)	~50 (1 wt%)	~95	Improved long-term resistance in saline media via synergistic combination of ZnO as well as SiO_2 nanoparticles embedded an epoxy matrix. Highlights the optimal loading is critical to prevent agglomeration.
ZnO/polymer nanocomposites (Quadri et al., 2017)	–	> Polymers alone	ZnO/polymer nanocomposites showed superior corrosion inhibition compared to pure polymers; inhibition mainly due to mixed physisorption and chemisorption mechanisms. Current study benefits from inorganic oxide synergy in a non-polymer matrix.
Nano-SiO_2 coating on galvanized steel (Liang et al., 2021)	–	Improved corrosion resistance	Enhances hydrophobicity and physical barrier properties. The present work builds on this by adding ZnO for active chemical passivation.
SiO_2 nanoparticles in plating (Xijing and Yong, 2023)	–	Enhanced cathodic protection	SiO_2 inclusion increases cathode current and coating hardness, indirectly boosting corrosion resistance through mechanical integrity.
Mixed-oxide nanocomposite systems (Baronins et al., 2023)	–	High	Corroborates that binary oxide systems (like SiO_2/ZnO) offer enhanced protection due to concurrent physical shielding and surface passivation.

is ascribed to the dual-action mechanism of the composite: SiO_2 acts as an inert, insulating layer minimizing electrolyte penetration, while ZnO adds passivating characteristics and electrochemical stability. The composite system thus creates a more robust and compact barrier that effectively impedes both anodic and cathodic processes on the metal surface .These findings clearly exhibit that the SiO_2/ZnO composite significantly enhances corrosion resistance over individual oxides, making it a promising candidate for protective coating applications in corrosive environments. These findings align with previous literature, supporting the efficiency of mixed-oxide nanocomposite systems in corrosion inhibition (Baronins et al., 2023). The following table depicts the comparisons of corrosion inhibition performance with respect to current study (Table 5).

This comparison shows that while other researchers have demonstrated corrosion inhibition via ZnO and SiO_2 nanoparticles or their combinations, the current study quantifies these benefits with detailed electrochemical parameters, highlighting superior inhibition efficiency and barrier properties supported by complementary mechanisms.

4. CONCLUSIONS

In conclusion, ZnO, SiO_2, and ZnO-SiO_2 nanocomposites were successfully synthesized and characterized, confirming the retention of ZnO's crystalline wurtzite structure within an amorphous silica matrix, and resulting in well-dispersed, mesoporous nanocomposite. Optical analysis indicated a widened band gap in the composite due to quantum confinement and silica interactions. Corrosion studies showed that all oxide coatings enhanced the protection of mild steel in acidic media, with the ZnO-SiO_2 nanocomposite achieving the highest inhibition efficiency (93%). This superior performance is attributed to a synergistic effect, combining the physical barrier properties of the SiO_2 matrix with the chemical passivation capabilities of the embedded ZnO nanoparticles.

5. ACKNOWLEDGEMENT

The authors want to grateful to the Department of Chemistry, College of Science at the University of Babylon that supported the laboratory infrastructure and technical assistance during the course of the given study. Special thanks are extended to the University of Tehran for SEM analysis and to the Ministry of Science and Technology for XRD measurements. The authors also appreciate the valuable guidance and constructive feedback from academic colleagues, as well as the assistance of laboratory staff in sample preparation and characterization.

REFERENCES

A., P. and J. R. Xavier (2025). A Review on Functional Nanocomposites for Enhanced Anticorrosion and Flame Retardant Properties. *Surfaces and Interfaces*, **70**; 106850

Abdus Samad, U., M. A. Alam, A. Anis, E. S. M. Sherif, S. I. Al-Mayman, and S. M. Al-Zahrani (2020). Effect of Incorporated ZnO Nanoparticles on the Corrosion Performance of SiO_2 Nanoparticle-Based Mechanically Robust Epoxy Coatings. *Materials*, **13**(17); 3767

Adam, R. E., G. Pozina, M. Willander, and O. Nur (2018). Synthesis of ZnO Nanoparticles by Co-Precipitation Method for Solar-Driven Photodegradation of Congo Red Dye at Different pH. *Photonics and Nanostructures – Fundamentals and Applications*, **32**; 11–18

Ahsbahs, H. and H. Sowa (2006). High-Pressure X-Ray Investigation of Zincite ZnO Single Crystals Using Diamond Anvils with an Improved Shape. *Journal of Applied Crystallography*, **39**(2); 169–175

Ajobree, A. M., A. T. Bader, A. F. Alkaim, and F. H. Hussein (2019). ZnO Nanoparticles as a Model for Removal of Pharmaceutical Compounds (Vitamin B12) in the Presence of UVA Light. *International Journal of Recent Technology and Engineering*, **8**(2S3); 1406–1409

Ali, A. M., A. A. Ismail, R. Najmy, and A. Al-Hajry (2014). Preparation and Characterization of ZnO-SiO_2 Thin Films as Highly Efficient Photocatalyst. *Journal of Photochemistry and Photobiology A: Chemistry*, **275**; 37–46

Andrade-Guel, M., C. Cabello-Alvarado, P. Bartolo-Pérez, D. I. Medellin-Banda, C. A. Ávila-Orta, B. Cruz-Ortiz, and G. Cadenas-Pliego (2022). Surface Modification of TiO_2/ZnO Nanoparticles by Organic Acids with Enhanced Methylene Blue and Rhodamine B Dye Adsorption Properties. *RSC Advances*, **12**(44); 28494–28504

Aslam, R., M. Mobin, Huda, I. B. Obot, and A. H. Alamri (2020). Ionic Liquids Derived from α-Amino Acid Ester Salts as Potent Green Corrosion Inhibitors for Mild Steel in 1 M HCl. *Journal of Molecular Liquids*, **318**; 113982

Babu, K. S., A. R. Reddy, K. V. Reddy, and A. N. Mallika (2014). High Thermal Annealing Effect on Structural and Optical Properties of ZnO-SiO_2 Nanocomposite. *Materials Science in Semiconductor Processing*, **27**; 643–648

Bahmani, S. H., B. B. K. Huat, A. Asadi, and N. Farzadnia (2014). Stabilization of Residual Soil Using SiO_2 Nanoparticles and Cement. *Construction and Building Materials*, **64**; 350–359

Baronins, J., M. Antonov, V. Abramovskis, A. Rautmane, V. Lapkovskis, I. Bockovs, and A. Shishkin (2023). The Effect of Zinc Oxide on DLP Hybrid Composite Manufacturability and Mechanical-Chemical Resistance. *Polymers*, **15**(24); 4679

Brus, L. E. (1984). Electron-Electron and Electron-Hole Interactions in Small Semiconductor Crystallites: The Size Dependence of the Lowest Excited Electronic State. *The Journal of Chemical Physics*, **80**(9); 4403–4409

Chen, Y., H. Ding, and S. Sun (2017). Preparation and Characterization of ZnO Nanoparticles Supported on Amorphous SiO_2. *Nanomaterials*, **7**(8); 217

Chen, Z., J. Wang, H. Wu, J. Yang, Y. Wang, J. Zhang, and Z. Tang (2022a). A Transparent Electrode Based on Solution-Processed ZnO for Organic Optoelectronic Devices. *Nature Communications*, **13**(1); 4387

Chen, Z. Y., W. Z. Shao, W. J. Li, X. Y. Sun, L. Zhen, and Y. Li (2022b). Suppressing the Agglomeration of ZnO Nanoparticles in Air by Doping with Lower Electronegativity Metallic Ions: Implications for Ag/ZnO Electrical Contact Composites. *ACS Applied Nano Materials*, **5**(8); 10809–10817

Corrales-Luna, M., T. Le Manh, M. Romero-Romo, M. Palomar-Pardavé, and E. M. Arce-Estrada (2019). 1-Ethyl-3-Methylimidazolium Thiocyanate Ionic Liquid as Corrosion Inhibitor of API 5L X52 Steel in H_2SO_4 and HCl Media. *Corrosion Science*, **153**; 85–99

Dey, S., D. L. Mohanty, N. Divya, V. Bakshi, A. Mohanty, D. Rath, and R. Sabui (2025). A Critical Review on Zinc Oxide Nanoparticles: Synthesis, Properties and Biomedical Applications. *Intelligent Pharmacy*, **3**(1); 53–70

Dhaffouli, A., M. Holzinger, S. Carinelli, H. Barhoumi, and P. A. Salazar-Carballo (2024). ZnO@SiO_2 Nanoparticles for Enhanced Electrochemical Detection of Cd^{2+} Ions in Real Samples. *Sensors*, **24**(13); 4179

Divya, M., B. Vaseeharan, M. Abinaya, S. Vijayakumar, M. Govindarajan, N. S. Alharbi, and G. Benelli (2018). Biopolymer Gelatin-Coated ZnO Nanoparticles Showed

High Antibacterial, Antibiofilm and Anti-Angiogenic Activity. *Journal of Photochemistry and Photobiology B: Biology*, **178**; 211–218

Dubey, R. S., Y. B. R. D. Rajesh, and M. A. More (2015). Synthesis and Characterization of SiO_2 Nanoparticles via Sol–Gel Method for Industrial Applications. *Materials Today: Proceedings*, **2**(4); 3575–3579

Fatimah, I., G. Fadillah, I. Sahroni, A. Kamari, S. Sagadevan, and R.-A. Doong (2021). Nanoflower-Like Composites of ZnO/SiO_2 Synthesized Using Bamboo Leaves Ash as Reusable Photocatalyst. *Arabian Journal of Chemistry*, **14**(3); 102973

Ghafouri, V., A. Ebrahimzad, and M. Shariati (2013). The Effect of Annealing Time and Temperature on Morphology and Optical Properties of ZnO Nanostructures Grown by a Self-Assembly Method. *Scientia Iranica*, **20**(3); 1039–1048

Grigorie, A. C., C. Muntean, T. Vlase, C. Locovei, and M. Stefanescu (2017). $ZnO-SiO_2$ Based Nanocomposites Prepared by a Modified Sol-Gel Method. *Materials Chemistry and Physics*, **186**; 399–406

Gupta, A., J. Verma, and D. Kumar (2023a). Mitigation of Erosion and Corrosion of Steel Using Nano-Composite Coating: Polyurethane Reinforced with SiO_2-ZnO Core–Shell Nanoparticles. *Progress in Organic Coatings*, **183**; 107733

Gupta, R., R. Verma, S. Kango, A. Constantin, P. Kharia, R. Saini, and P. Chamoli (2023b). A Critical Review on Recent Progress, Open Challenges, and Applications of Corrosion-Resistant Superhydrophobic Coating. *Materials Today Communications*, **34**; 105201

Heinhold, R., G. T. Williams, S. P. Cooil, D. A. Evans, and M. W. Allen (2013). Influence of Polarity and Hydroxyl Termination on the Band Bending at ZnO Surfaces. *Physical Review B*, **88**(23); 235315

Huang, D., Y. Zhang, J. Zhang, H. Wang, M. Wang, C. Wu, and Z. Zhao (2019). The Synergetic Effect of a Structure-Engineered Mesoporous SiO_2-ZnO Composite for Doxycycline Adsorption. *RSC Advances*, **9**(66); 38772–38782

Joni, I. M., Rukiah, and C. Panatarani (2020). Synthesis of Silica Particles by Precipitation Method of Sodium Silicate: Effect of Temperature, pH and Mixing Technique. *AIP Conference Proceedings*, **2219**(1); 020043

Justine, M., H. Joy Prabu, I. Johnson, D. Magimai Antoni Raj, S. John Sundaram, and K. Kaviyarasu (2021). Synthesis and Characterization Studies of ZnO and $ZnO-SiO_2$ Nanocomposite for Biodiesel Applications. *Materials Today: Proceedings*, **36**; 440–446

Kamat, P. V. (2007). Meeting the Clean Energy Demand: Nanostructure Architectures for Solar Energy Conversion. *The Journal of Physical Chemistry C*, **111**(7); 2834–2860

Krishnakumar, B., A. Balakrishna, S. A. Nawabjan, V. Pandiyan, A. Aguiar, and A. J. F. N. Sobral (2017). Solar and Visible Active Amino Porphyrin/SiO_2-ZnO for the Degradation of Naphthol Blue Black. *Journal of Physics and Chemistry of Solids*, **111**; 364–371

Kumar Yadav, V. and M. H. Fulekar (2019). Green Synthesis and Characterization of Amorphous Silica Nanoparticles from Fly Ash. *Materials Today: Proceedings*, **18**; 4351–4359

Li, J., Z. Liu, and Z. Wang (2023). Study of Nano-ZnO Improvement of the Mechanical Properties and Corrosion Resistance of Modified-SiO_2/PTFE Superhydrophobic Nanocomposite Coatings by One-Step Spraying. *New Journal of Chemistry*, **47**(13); 6246–6257

Liang, T., H. Yuan, C. Li, S. Dong, C. Zhang, G. Cao, and X. Cao (2021). Corrosion Inhibition Effect of Nano-SiO_2 for Galvanized Steel Superhydrophobic Surface. *Surface and Coatings Technology*, **406**; 126673

Liang, Y., J. Ouyang, H. Wang, W. Wang, P. Chui, and K. Sun (2012). Synthesis and Characterization of Core-Shell Structured SiO_2@YVO_4:Yb^{3+},Er^{3+} Microspheres. *Applied Surface Science*, **258**(9); 3689–3694

Mishra, P. K., H. Mishra, A. Ekielski, S. Talegaonkar, and B. Vaidya (2017). ZnO Nanoparticles: A Promising Nanomaterial for Biomedical Applications. *Drug Discovery Today*, **22**(12); 1825–1834

Nam, N. H. and N. H. Luong (2019). Nanoparticles: Synthesis and Applications. In V. Grumezescu and A. M. Grumezescu, editors, *Materials for Biomedical Engineering*. Elsevier, pages 211–240

Nguyen, T. H., T. C. Vu, T. P. Le, T. H. Nguyen, X. T. Do, and A. T. Vu (2024). Synthesis of Mesoporous $ZnO \cdot SiO_2$ Nanocomposite from Rice Husk for Enhanced Degradation of Organic Substances Including Janus Green B under Visible Light. *Bulletin of Chemical Reaction Engineering & Catalysis*, **19**(1); 20175

Özgür, Ü., Y. I. Alivov, C. Liu, A. Teke, M. A. Reshchikov, S. Doğan, V. Avrutin, S.-J. Cho, Morkoç, and H (2005). A comprehensive review of ZnO materials and devices. *Journal of applied physics*, **98**(4)

Peng, Q. Q., M. Liu, Y. F. Huang, G. Z. Ma, W. L. Guo, H. D. Wang, and Z. G. Xing (2023). Preparation and Properties of Al_2O_3-PF Composite Functional Protective Coating on the Surface of Polymer Matrix Composites. *Surface and Coatings Technology*, **456**; 129138

Prošek, T., P. Keil, and K. Popova (2025). Corrosion Protection and Sustainability: Why Are the Two Concepts Inherently Intertwined. *Corrosion and Materials Degradation*, **6**(3); 38

Quadri, T., L. Olasunkanmi, O. Fayemi, M. Solomon, and E. Ebenso (2017). ZnO Nanocomposites of Selected Polymers: Synthesis, Characterization, and Corrosion Inhibition Studies on Mild Steel in HCl Solution. *ACS Omega*, **2**(12); 8421–8437

Rahmat, F. I., Y. W. Fen, M. F. Anuar, N. A. S. Omar, M. H. M. Zaid, K. A. Matori, and R. E. M. Khaidir (2021). Synthesis and Characterization of $ZnO-SiO_2$ Composite Using Oil Palm Empty Fruit Bunch as a Potential Silica Source. *Molecules*, **26**(4); 1061

Raji, S. Q. and A. T. Bader (2025). Synthesis and Characterization of Co_3O_4 and ZnO Nanoparticles Based on Schiff Base Complexes as a Precursor to the Photocatalytic Pho-

todegradation of Congo Red Dye. *Science and Technology Indonesia*, **10**(2); 420–431

Raza, A., A. Ashraf, S. Ali, F. Bashir, M. A. Farrukh, F. Naseem, and D. E. Shahwar (2025). Assessing the Impact of NaOH on Green Synthesis of Zinc-Based Nanoparticles Using Onion Extract and Exploring Their Photocatalytic, Antibacterial, and Antioxidant Potentials. *ChemistrySelect*, **10**(23); e00253

S., M., H. N., and V. P. P. (2020). In Vitro Biocompatibility and Antimicrobial Activities of ZnO Nanoparticles (ZnO NPs) Prepared by Chemical and Green Synthetic Route: A Comparative Study. *BioNanoScience*, **10**(1); 112–121

Safavinia, L., M. R. Akhgar, B. Tahamipour, and S. A. Ahmadi (2021). Green Synthesis of Highly Dispersed ZnO Nanoparticles Supported on Silica Gel Matrix by Daphne oleoides Extract and Their Antibacterial Activity. *Iranian Journal of Biotechnology*, **19**(1); 86–95

Samuel, A., A. Abdullah, G. Xavier, S. Stephen, M. M. Zeidan, D. Choi, and S. Abedrabbo (2025). Sol–Gel Synthesis and Characterization of ZnO−SiO_2 Nanocomposites: A Comparative Study with Pure ZnO and SiO_2. *Nanoscale Advances*, **7**(22); 7145–7155

Singh, R., M. S. Smitha, and S. P. Singh (2014). The Role of Nanotechnology in Combating Multi-Drug Resistant Bacteria. *Journal of Nanoscience and Nanotechnology*, **14**(7); 4745–4756

Skuja, L. (1998). Optically Active Oxygen-Deficiency-Related Centers in Amorphous Silicon Dioxide. *Journal of Non-Crystalline Solids*, **239**(1); 16–48

Spanhel, L. and M. A. Anderson (1991). Semiconductor Clusters in the Sol–Gel Process: Quantized Aggregation, Gelation, and Crystal Growth in Concentrated ZnO Colloids. *Journal of the American Chemical Society*, **113**(8); 2826–2833

Subhi, H. M., A. T. Bader, and H. Y. Al-Gubury (2022). Synthesis and Characterization of ZnO Nanoparticles via Thermal Decomposition for Zn(II) Schiff Base Complex. *Indonesian Journal of Chemistry*, **22**(5); 1396–1406

Sukhov, I., I. Filippov, I. Pronin, V. Sysoev, V. Kondratev, A. Komolov, and G. Korotcenkov (2024). Sol–Gel Prepared ZnO: UV Irradiation Effect on Structure and Surface Properties. *Mendeleev Communications*, **34**; 643–646

Tan, S. T., B. J. Chen, X. W. Sun, W. J. Fan, H. S. Kwok, X. H. Zhang, and S. J. Chua (2005). Blueshift of Optical Band Gap in ZnO Thin Films Grown by Metal-Organic Chemical Vapor Deposition. *Journal of Applied Physics*, **98**(1); 013505

Tauc, J. (2012). *Amorphous and Liquid Semiconductors*. Springer US, Boston, MA

Thirumalaivasan, N., S. Nangan, A. MariaJoseph, and K. Kanagaraj (2025). Advancements in Hybrid Silica Nanoparticles for Pioneering Precision in Targeted Drug Delivery and Diagnostic Applications. *Next Nanotechnology*, **8**; 100298

Top, A. and H. Çetinkaya (2015). Zinc Oxide and Zinc Hydroxide Formation via Aqueous Precipitation: Effect of the Preparation Route and Lysozyme Addition. *Materials Chemistry and Physics*, **167**; 77–87

Torkian, P., S. M. Najafabadi, A. Szuławska-Mroczek, D. Grzelczyk, and M. Ghashang (2024). Al-Doped ZnO/-SiO_2 Nano-Glass Ceramic System: A New Composite System for Improvement in Thermal Stability and Mechanical Properties of Dental Resins. *Journal of Materials Engineering and Performance*, **33**(24); 14463–14470

Xijing, L. and C. Yong (2023). Effect of SiO_2 Nanoparticles on the Hardness and Corrosion Resistance of NiW/SiO_2 Nanocomposite Coating Prepared by Electrodeposition. *International Journal of Electrochemical Science*, **18**(6); 100138

Yang, G., Q. Guo, D. Yang, P. Peng, and J. Li (2019). Disperse Ultrafine Amorphous SiO_2 Nanoparticles Synthesized via Precipitation and Calcination. *Colloids and Surfaces A: Physicochemical and Engineering Aspects*, **568**; 445–454

Yang, H., Y. Xiao, K. Liu, and Q. Feng (2008). Chemical Precipitation Synthesis and Optical Properties of ZnO/SiO_2 Nanocomposites. *Journal of the American Ceramic Society*, **91**(5); 1591–1596

Zhang, J., Q. Xu, Z. Feng, M. Li, and C. Li (2008). Importance of the Relationship between Surface Phases and Photocatalytic Activity of TiO_2. *Angewandte Chemie International Edition*, **47**(9); 1766–1769

Zhang, L., Y. Jiang, Y. Ding, N. Daskalakis, L. Jeuken, M. Povey, and D. W. York (2010). Mechanistic Investigation into Antibacterial Behaviour of Suspensions of ZnO Nanoparticles against *E. coli*. *Journal of Nanoparticle Research*, **12**(5); 1625–1636

Zhang, Y., M. Kang, L. Yao, N. S. Mbugua, M. Jin, and J. Zhu (2020). Study on the Wear and Seawater Corrosion Resistance of Ni−Co−P Alloy Coatings with Jet Electrodeposition at Different Jet Voltages and Plating Solution Temperatures. *Coatings*, **10**(7); 639

